

1 Effects of aquifer geometry on seawater intrusion in annulus
2 segment island aquifers

3
4 Zhaoyang Luo^{1,2}, Jun Kong^{1,3,#}, Chengji Shen¹, Pei Xin¹, Chunhui Lu¹, Ling Li⁴,
5 David Andrew Barry²

6
7 ¹State Key Laboratory of Hydrology-Water Resources and Hydraulic Engineering, Hohai
8 University, Nanjing, China

9
10 ²Ecological Engineering Laboratory (ECOL), Environmental Engineering Institute (IIE),
11 Faculty of Architecture, Civil and Environmental Engineering (ENAC), École Polytechnique
12 Fédérale de Lausanne (EPFL), Lausanne, Switzerland

13
14 ³Jiangsu Key Laboratory of Coast Ocean Resources Development and Environment Security,
15 Hohai University, Nanjing, China

16
17 ⁴School of Engineering, Westlake University, Hangzhou, China

18
19 [#]Corresponding author: Jun Kong (kongjun999@126.com)

20
21 Resubmitted to *Hydrology and Earth System Sciences* on 26 November 2021

22 **Abstract**

23 Seawater intrusion in island aquifers was considered analytically, specifically for annulus
24 segment aquifers (ASAs), i.e., aquifers that (in plan) have the shape of an annulus segment.
25 Based on the Ghijben-Herzberg and hillslope-storage Boussinesq equations, analytical
26 solutions were derived for steady-state seawater intrusion in ASAs, with a focus on the
27 freshwater-seawater interface and its corresponding watertable elevation. Predictions of the
28 analytical solutions compared well with experimental data, and so they were employed to
29 investigate the effects of aquifer geometry on seawater intrusion in island aquifers. Three
30 different ASA geometries were compared: convergent (smaller side facing the lagoon, larger
31 side is the internal no-flow boundary, flow converges towards the lagoon), rectangular and
32 divergent (smaller side is the internal no-flow boundary, larger side facing the sea, flow
33 diverges towards the sea). Depending on the aquifer geometry, seawater intrusion was found
34 to vary greatly, such that the assumption of a rectangular aquifer to model an ASA can lead to
35 poor estimates of seawater intrusion. Other factors being equal, compared with rectangular
36 aquifers, seawater intrusion is more extensive and watertable elevation is lower in divergent
37 aquifers, with the opposite tendency in convergent aquifers. Sensitivity analysis further
38 indicated that the effects of aquifer geometry on seawater intrusion and watertable elevation
39 vary with aquifer width and distance from the circle center to the inner arc (the lagoon
40 boundary for convergent aquifers or the internal no-flow boundary for divergent aquifers). A
41 larger aquifer width and distance from the circle center to the inner arc weaken the effects of
42 aquifer geometry and hence differences in predictions for the three geometries become less

43 pronounced.

44 **Keywords:** sharp-interface; steady-state analytical solution; atoll aquifer; annulus segment
45 aquifer, seawater intrusion

46 **Key Points**

47 ➤ Analytical solutions of steady-state seawater intrusion were derived for annulus segment
48 aquifers

49 ➤ Among three different aquifer geometries, divergent aquifers have the lowest watertable
50 and hence the most extensive seawater intrusion

51 ➤ Aquifer geometry effects on seawater intrusion depend on the aquifer width and distance
52 from the circle center to the inner arc

53 1. Introduction

54 Islands are extensively distributed throughout the world's oceans. Unfortunately, their
55 groundwater resources are impacted by sea-level rise and increased demands. According to a
56 recent estimate, there are approximately 65 million people living in oceanic islands where
57 groundwater may be the only source of freshwater (Thomas et al., 2020). Fresh groundwater
58 stored on oceanic islands is mainly from precipitation (usually in the form of a freshwater
59 lens) and its availability varies due to different factors, e.g., island topography, rainfall
60 patterns, tides, episodic storms and human activities (White & Falkland, 2010; Storlazzi et al.,
61 2018). Seawater intrusion is thus an important issue due to its deleterious effect on oceanic
62 island freshwater storage (e.g., Werner et al., 2017; Lu et al., 2019; Memari et al., 2020).

63 Over the past few decades, seawater intrusion in oceanic islands has been extensively
64 investigated in field observations (e.g., Röper et al., 2013; Post et al., 2019), laboratory
65 experiments (e.g., Stoeckl et al., 2015; Bedekar et al., 2019; Memari et al., 2020), numerical
66 simulations (e.g., Lam, 1974; Gingerich et al., 2017; Liu & Tokunaga, 2019) and analytical
67 solutions (e.g., Fetter, 1972; Ketabchi et al., 2014; Lu et al., 2019). Among these, analytical
68 solutions are effective tools to assess the extent of seawater intrusion (i.e., the location of the
69 freshwater-seawater interface), although they cannot incorporate complex factors (e.g.,
70 dispersive mixing and transient oceanic dynamics) (Werner et al., 2013). The advantages of
71 analytical solutions are that they are computationally efficient, can be used as test cases for
72 numerical models, and can reveal the explicit relationships between parameters that influence
73 seawater intrusion (e.g., Fetter, 1972; Ketabchi et al., 2014; Liu et al., 2014; Lu et al., 2019).

74 Based on the Dupuit-Forchheimer approximation (i.e., ignoring vertical flow) and the
75 Ghijben-Herzberg equation (Drabbe & Badon Ghijben, 1889, English translation given by
76 Post (2018); Herzberg, 1901), Fetter (1972) presented analytical solutions describing the
77 freshwater-seawater interface location and watertable elevation in a circular island. Bailey et
78 al. (2010) further compared these single-layered analytical solutions with field measurements,
79 indicating that the analytical solutions perform well in estimating the freshwater-seawater
80 interface location and watertable elevation. Fetter's solutions formed the foundation for many
81 subsequent analytical studies on seawater intrusion in island aquifers. Again, for a single
82 layer, Chesnaux and Allen (2008) and Greskowiak et al. (2013) developed analytical solutions
83 to predict the steady-state groundwater age distribution in freshwater lenses. In addition, using
84 single-layered analytical solutions, Morgan and Werner (2014) proposed vulnerability
85 indicators of freshwater lenses under sea-level rise and recharge change.

86 Since aquifers are usually heterogeneous, the single-layer analytical solutions were
87 subsequently extended to two-layered island aquifers. Vacher (1988) derived solutions for the
88 freshwater-seawater interface location and watertable elevation for infinite-strip islands
89 composed of different layers. Dose et al. (2014) conducted laboratory experiments to validate
90 and confirm the reliability of analytical solutions proposed by Fetter (1972) and Vacher
91 (1988). Ketabchi et al. (2014) extended Fetter's analytical solutions to calculate the
92 freshwater-seawater interface location and watertable elevation in two-layered circular islands
93 subject to sea-level rise. Their results indicated that land-surface inundation caused by sea-
94 level rise has a considerable impact on fresh groundwater lenses. Recently, Lu et al. (2019)

95 derived analytical solutions for the freshwater-seawater interface location and watertable
96 elevation for both strip and circular islands with two adjacent layers, i.e., a less permeable
97 slice along the shoreline of an island, and a more permeable zone inland.

98 All the abovementioned analytical solutions apply to either strip or circular islands.

99 According to the classification of sand dunes developed by Stuyfzand (1993; 2017), there are
100 different island layouts that should be considered, e.g., where the shape of the island is an
101 annulus segment, instead of a strip or circular disk (Figure 1). Annulus segment-shaped
102 islands are found in various atolls (i.e., circular chains of islands surrounding a central
103 lagoon) as found in the Pacific and Indian Oceans (Werner et al., 2017; Duvat, 2019).

104 Nevertheless, analytical solutions of seawater intrusion are not yet available for annulus
105 segment aquifers (ASAs). In general, ASAs are conceptually treated as a 2D cross section,
106 similar to strip islands (e.g., Ayers & Vacher, 1986; Underwood et al., 1992; Bailey et al.,
107 2009; Werner et al., 2017). Evidently, topography plays an important role in groundwater flow
108 and hence seawater intrusion (e.g., Zhang et al., 2016; Liu & Tokunaga, 2019). It remains
109 unclear whether analytical solutions of seawater intrusion for strip islands are appropriate for
110 ASAs. It is also unclear how island geometry affects the freshwater-seawater interface
111 location and watertable elevation of ASAs.

112 In this study, analytical solutions are derived for steady-state seawater intrusion for ASAs,
113 with a focus on the freshwater-seawater interface location and its corresponding watertable
114 elevation. After comparing their predictions with experimental data (Memari et al., 2020), the
115 analytical solutions are employed to investigate the effects of aquifer geometry on the

116 freshwater-seawater interface location and watertable elevation in ASAs.

117 **2. Conceptual Model**

118 Figure 2 shows the conceptual model of an ASA (a slice of an atoll island). The plan
119 view of the model domain is represented as a sector ($EF GH$) with an angle θ (Figure 2a).
120 The sea (EF) and lagoon (HG) boundaries are located at $L + L_0$ [L] and L_0 [L] from the circle
121 center, respectively. Since the longitudinal length is usually much longer than the lateral
122 length for an atoll island (Werner et al., 2017), seawater intrusion from the lateral sides (EH
123 and FG , Figure 2a) is negligible in comparison to the longitudinal side, especially for the
124 middle portion of an ASA. Therefore, EH and FG are treated as lateral no-flow boundaries.
125 Note that treating the lateral sides as no-flow boundaries is often used in studies of freshwater
126 lenses on atoll islands (e.g., Ayers & Vacher, 1986; Underwood et al., 1992; Bailey et al.,
127 2009; Werner et al., 2017). The lateral vertical cross section of the model domain is
128 conceptualized as a rectangle ($ABCD$) along the radial direction with dimensions of L [L]
129 (width) \times d [L] (height) (Figure 2b, c). AD is the impermeable base while BC is the land
130 surface through which aquifer recharge flows.

131 Both the sea and lagoon water levels are set to H_s [L], which results in an internal no-
132 flow boundary (water divide, where the slope of the watertable is zero) between the sea and
133 lagoon (location of the z -axis in Figure 2b,c). The segment between the sea and the internal
134 no-flow boundary is referred to as Unit 1, whereas the segment between the internal no-flow
135 and lagoon boundaries is referred to as Unit 2 (Figure 2). The widths of Units 1 and 2 are l_1
136 [L] and l_2 [L], respectively. In addition, the flow is asymmetrical in Units 1 and 2, with

137 divergent flow (the aquifer length w [L] increases along the flow direction) in Unit 1 and
138 convergent flow (w decreases along the flow direction) in Unit 2.

139 The r - z coordinate origin is placed at the intersection of the internal no-flow boundary
140 and impermeable base, with the r -axis pointing to the circle center (radial direction) and the z -
141 axis pointing vertically upward. Further, ϕ [L] is the watertable height, h [L] is the
142 vertical distance between the watertable and the interface, h_s [L] is the vertical distance
143 between the sea level and the interface, and $h_c = H_s - h_s$ [L] is the vertical distance from the
144 impermeable base to the interface for given r (Figure 2b,c). Constant recharge into the
145 saturated zone, N [LT⁻¹], is assumed. There are two possibilities for the interface tip (i.e., the
146 location where the freshwater-seawater interface connects to the z -axis or the bottom
147 boundary): above the aquifer bed (Figure 2b) or on the aquifer bed (Figure 2c). The r -
148 coordinates of the interface tip in Units 1 and 2 are denoted as r_{t1} [L] and r_{t2} [L], respectively
149 (Figure 2c). Note that $r_{t1} = r_{t2} = 0$ when the interface tip is above the aquifer bed, as in Figure
150 2b.

151 Consistent with previous studies (e.g., Ketabchi et al., 2014; Lu et al., 2016; 2019), the
152 following assumptions are made: (1) steady-state flow, (2) sharp freshwater-seawater
153 interface, (3) homogeneous and isotropic aquifer with a horizontal bottom, (4) rainfall is equal
154 to the replenishment of the saturated zone with a magnitude that is less than the saturated
155 hydraulic conductivity (else overland flow will appear), (5) vertical flow in the saturated zone
156 is negligible (the Dupuit-Forchheimer approximation), and (6) the same velocity is assumed
157 on the arc (w) for a given radial distance r , leading to radial flow only. Based on this last

158 assumption, the 3D flow problem can be simplified to 1D, making it possible to consider
159 geometry effects analytically (Fan & Bras, 1998; Paniconi et al., 2003; Troch et al., 2003).

160 **3. Analytical Solutions**

161 Under the abovementioned assumptions, groundwater flow in an ASA (Figure 2) can be
162 described as (Fan & Bras, 1998; Paniconi et al., 2003; Troch et al., 2003),

$$163 \quad -\frac{d}{dr}(wq) + Nw = 0 \quad (1)$$

164 where q [L^2T^{-1}] is the radial flux per unit length along the radial direction r [L]. Equation
165 (1) is a special case of the hillslope-storage Boussinesq equation proposed by Troch et al.

166 (2003). Paniconi et al. (2003) validated the hillslope-storage Boussinesq equation by

167 comparing it with a 3D Richards' equation model and found that predictions of the hillslope-

168 storage Boussinesq equation matched well those of the 3D model for seven different

169 geometries. For conciseness, readers are referred to Paniconi et al. (2003) for more details

170 about the validation. Subsequently, the hillslope-storage Boussinesq equation was used to for

171 different analyses (Hilberts et al., 2005, 2007; Hazenberg et al., 2015, 2016; Kong et al.,

172 2016; Luo et al., 2018), all of which focus on hillslope aquifers where the aquifer bottom is

173 usually sloping. The hillslope-storage Boussinesq equation assumes that groundwater flow is

174 parallel to the aquifer bottom (the Dupuit-Forchheimer approximation). Therefore, it can be

175 applied to coastal unconfined aquifers where the aquifer bottom slope is usually mild (Lu et

176 al., 2016).

177 According to Darcy's law and the Dupuit-Forchheimer approximation, the freshwater

178 flux in the aquifer segment between the seaward boundary and interface tip can be calculated

179 as (ϕ is independent of z),

$$180 \quad q = -\int_{h_c}^{\phi} K_s \frac{d\phi}{dr} dz = -K_s (\phi - h_c) \frac{d\phi}{dr} \quad (2)$$

181 where K_s [LT^{-1}] is the saturated hydraulic conductivity.

182 **3.1. Interface Tip above the Aquifer Bed**

183 We first consider the situation where the interface tip is above the aquifer bed (Figure
184 2b). In Unit 1 where $w = \theta(L_0 + l_2 - r)$, substituting equation (2) into equation (1) and then
185 integrating gives,

$$186 \quad -\frac{1}{2} \left[(L_0 + l_2 - r)^2 - (L_0 + l_2)^2 \right] N = -(L_0 + l_2 - r) K_s (\phi - h_c) \frac{d\phi}{dr} \quad (3)$$

187 According to the Ghijben-Herzberg equation, the vertical thickness of the freshwater zone (h)
188 in the interface zone is given by,

$$189 \quad h = \phi - h_c = (1 + \alpha)(\phi - H_s) \quad (4)$$

190 where $\alpha = \rho_f / (\rho_s - \rho_f)$ is the dimensionless density difference, and ρ_f [ML^{-3}] and ρ_s

191 [ML^{-3}] are the freshwater and seawater densities, respectively. Substitution of equation (4)

192 into equation (3) yields,

$$193 \quad -\frac{1}{2} \left[(L_0 + l_2 - r)^2 - (L_0 + l_2)^2 \right] N = -K_s (L_0 + l_2 - r) (1 + \alpha) (\phi - H_s) \frac{d\phi}{dr} \quad (5)$$

194 Rearranging equation (5) produces,

$$195 \quad -\frac{(L_0 + l_2 - r)N}{2} + \frac{N(L_0 + l_2)^2}{2(L_0 + l_2 - r)} = -K_s (1 + \alpha) (\phi - H_s) \frac{d\phi}{dr} \quad (6)$$

196 Integrating equation (6) leads to,

$$197 \quad -\frac{(L_0 + l_2)^2 N}{2} \ln(L_0 + l_2 - r) - \frac{1}{2}(L_0 + l_2)Nr + \frac{1}{4}Nr^2 + C_1 = -K_s (1 + \alpha) \frac{(\phi - H_s)^2}{2} \quad (7)$$

198 where C_1 is the integration constant that is determined by the sea boundary condition (i.e.,

199 $r = -l_1, \phi = H_s$,

200
$$C_1 = \frac{(L_0 + l_2)^2 N}{2} \ln(L_0 + l_2 + l_1) - \frac{1}{2}(L_0 + l_2)l_1 N - \frac{1}{4}l_1^2 N \quad (8)$$

201 The relation between h_s and ϕ is given by,

202
$$h_s = \alpha(\phi - H_s) \quad (9)$$

203 Combining equation (7) with equation (9) and eliminating ϕ yields,

204
$$-\frac{(L_0 + l_2)^2 N}{2} \ln(L_0 + l_2 - r) - \frac{1}{2}(L_0 + l_2)Nr + \frac{1}{4}Nr^2 + C_1 = -K_s(1 + \alpha)\frac{h_s^2}{2\alpha^2} \quad (10)$$

205 Equation (10) gives the freshwater-seawater interface location in Unit 1 once l_1 and l_2 are
206 determined.

207 Equation (7) applies to Unit 2 by replacing C_1 with C_2 ,

208
$$-\frac{(L_0 + l_2)^2 N}{2} \ln(L_0 + l_2 - r) - \frac{1}{2}(L_0 + l_2)Nr + \frac{1}{4}Nr^2 + C_2 = -K_s(1 + \alpha)\frac{(\phi - H_s)^2}{2} \quad (11)$$

209 where C_2 is chosen to satisfy the lagoon boundary condition ($r = l_2, \phi = H_s$),

210
$$C_2 = \frac{(L_0 + l_2)^2 N}{2} \ln(L_0) + \frac{1}{2}(L_0 + l_2)l_2 N - \frac{1}{4}l_2^2 N \quad (12)$$

211 Combining equations (9) and (11) and eliminating ϕ leads to,

212
$$-\frac{(L_0 + l_2)^2 N}{2} \ln(L_0 + l_2 - r) - \frac{1}{2}(L_0 + l_2)Nr + \frac{1}{4}Nr^2 + C_2 = -K_s(1 + \alpha)\frac{h_s^2}{2\alpha^2} \quad (13)$$

213 Equation (13) gives the freshwater-seawater interface location in Unit 2 once l_2 is
214 determined. Since the sea level and lagoon water level are the same, an internal no-flow
215 boundary exists between the sea and lagoon, i.e.,

216
$$r = 0, (h_s)_{unit1} = (h_s)_{unit2} \quad (14)$$

217 where $(h_s)_{unit1}$ and $(h_s)_{unit2}$ represent h_s in Units 1 and 2, respectively.

218 Combining equations (10), (13) and (14) leads to expressions for l_1 and l_2 ,

$$219 \quad l_1 = L + L_0 - \sqrt{\frac{2LL_0 + L^2}{2\ln(L + L_0) - 2\ln(L_0)}} \quad (15)$$

$$220 \quad l_2 = \sqrt{\frac{2LL_0 + L^2}{2\ln(L + L_0) - 2\ln(L_0)}} - L_0 \quad (16)$$

221 As indicated by equations (15) and (16), the internal no-flow boundary between the sea and
 222 lagoon only depends on L and L_0 . For known l_1 and l_2 , equations (10) and (13) can be
 223 employed to predict the freshwater-seawater interface location in Units 1 and 2, respectively.

224 Once the interface location is determined, h and ϕ are given by,

$$225 \quad h = \frac{1 + \alpha}{\alpha} h_s \quad (17)$$

$$226 \quad \phi = \frac{h_s}{\alpha} + H_s \quad (18)$$

227 **3.2. Interface Tip on the Aquifer Bed**

228 When the interface tip is on the aquifer bed, the location of the internal no-flow
 229 boundary remains the same as for the interface tip above the aquifer bed. The freshwater-
 230 seawater interface for Units 1 and 2 can be determined by equations (10) and (13),
 231 respectively. Then, from equation (17), h at the aquifer segment between the sea boundary and
 232 the interface tip is determined. To calculate h for the aquifer segment between the interface tip
 233 and the internal no-flow boundary, the r -coordinate of the interface tip is found. At the
 234 interface tip of Unit 1 ($r = r_{t1}$),

$$235 \quad h_s = H_s \quad (19)$$

$$236 \quad \phi = \frac{1 + \alpha}{\alpha} H_s \quad (20)$$

237 With equations (10) and (20), r_{t1} is given by,

$$-\frac{(L_0 + l_2)^2 N}{2} \ln(L_0 + l_2 - r_{t1}) - \frac{1}{2}(L_0 + l_2)Nr_{t1} + \frac{1}{4}Nr_{t1}^2 = -C_1 - K_s(1 + \alpha)\frac{H_s^2}{2\alpha^2} \quad (21)$$

Let,

$$a = \frac{1}{4}N \quad (22a)$$

$$b = -\frac{1}{2}(L_0 + l_2)N \quad (22b)$$

$$c = -\frac{(L_0 + l_2)^2 N}{2} \quad (22c)$$

and

$$m = -C_1 - K_s(1 + \alpha)\frac{H_s^2}{2\alpha^2} \quad (22d)$$

then equation (21) becomes,

$$ar_{t1}^2 + br_{t1} + c \ln(L_0 + l_2 - r_{t1}) = m \quad (23)$$

which is solved by a root-finding method.

The freshwater discharge for the aquifer segment between the interface tip and the internal no-flow boundary is calculated as,

$$-\frac{1}{2}[(L_0 + l_2 - r)^2 - (L_0 + l_2)^2]N = -(L_0 + l_2 - r)K_s\phi\frac{d\phi}{dr} \quad (24)$$

Repeating the steps from equations (3) to (7) gives,

$$-\frac{(L_0 + l_2)^2 N}{2} \ln(L_0 + l_2 - r) - \frac{1}{2}(L_0 + l_2)Nr + \frac{1}{4}Nr^2 + C_3 = -\frac{K_s}{2}\phi^2 \quad (25)$$

where C_3 is determined by substituting equation (20) into equation (25). Then, equation (25) can be adopted to calculate h for the segment between the interface tip and the internal no-flow boundary where $h = \phi$.

Similarly, the r -coordinate of the interface tip in Unit 2 (r_{t2}) is obtained by substituting

257 equation (19) into equation (13). Then, the watertable (h) of the aquifer segment between the
258 interface tip and the internal no-flow boundary for Unit 2 is computed by repeating the steps
259 from equations (21) to (25).

260 **4. Results and Discussion**

261 **4.1. Validation of the Analytical Solutions**

262 The analytical solutions were validated by comparing their predictions with experimental
263 data compiled from Memari et al. (2020), who reported experiments carried out using a 15°
264 radial tank. The tank contained three distinct chambers: internal no-flow boundary condition,
265 porous medium and constant-head boundary condition (i.e., sea or lagoon). The internal no-
266 flow and seaward boundaries were respectively located at 10 and 55.5 cm from the circle
267 center, i.e., 45.5 cm from the internal no-flow boundary to the constant-head boundary along
268 the radial direction. Note that the experimental tank corresponds to Unit 1 of the radial aquifer
269 with $l_1 = 45.5$ cm and $l_2 = 0$, so the analytical results were calculated using equations (10)
270 and (23). The thicknesses of the porous medium and sea level were 28 and 25 cm,
271 respectively, with $K_s = 1.23 \times 10^{-2}$ m s⁻¹. The measured saltwater and freshwater densities
272 were respectively 1.015 and 0.999 g ml⁻¹, leading to $\alpha = 62$. Two different recharge events
273 with constant N , 2.46×10^{-4} and 1.08×10^{-4} m s⁻¹, were considered in the experiments.

274 Figure 3 shows the comparison between analytical and experimental results of the
275 freshwater-seawater interface for different recharge events. In general, the analytical solution
276 predicts the freshwater-seawater interface well for both recharge events, despite there being
277 some differences between the analytical results and the measurements, particularly in the zone

278 near the constant-head boundary ($r = -45$ cm). These deviations are likely due to assumptions
279 made in the analytical solution, i.e., (i) a sharp freshwater-seawater interface, (ii) ignoring the
280 effect of freshwater discharge, and (iii) neglecting the vertical flow (the Dupuit-Forchheimer
281 approximation).

282 **4.2. Effects of Aquifer Geometry on Seawater Intrusion**

283 Previous studies showed that boundary conditions play a critical role in estimates of
284 seawater intrusion (Werner & Simmons, 2009; Lu et al., 2016). Therefore, the internal no-
285 flow boundary between the sea and lagoon was examined for various ASAs. As indicated by
286 equations (15) and (16), this internal no-flow boundary depends only on L and L_0 . The values
287 of l_1 and l_2 calculated respectively from equations (15) and (16) are shown in Figure 4 for
288 three typical values of L (500, 1000 and 2000 m) with L_0 varying from 10^2 to 10^6 m. In
289 general, the internal no-flow boundary deviates from the middle of the ASA. When L_0 is less
290 than 10^5 m, l_1 is larger than l_2 for the three different values of L , indicating an internal no-
291 flow boundary closer to the lagoon boundary. For example, taking $L = 2000$ m and $L_0 = 100$ m
292 leads to $l_1 = 1240$ m and $l_2 = 760$ m, with a deviation of 240 m (12% of 2000 m) from the
293 middle of the ASA. When L_0 exceeds 10^5 m, however, the location of the internal no-flow
294 boundary can be approximated as being at the middle of the ASA for all considered values of
295 L . This is in contrast to strip and circular aquifers where the internal no-flow boundary is
296 always in the middle of aquifer due to symmetry.

297 Since the internal no-flow boundary location between the sea and lagoon deviates from
298 the middle of the ASA, we expect aquifer geometry to play a significant role in controlling

299 seawater intrusion. As mentioned previously, ASAs can be convergent (Unit 1) or divergent
300 aquifers (Unit 2) where the extent of seawater intrusion may be different. However, for strip
301 aquifers, both Units 1 and 2 are rectangular with the same extent of seawater intrusion.
302 Therefore, three geometries were compared in this study: convergent, rectangular and
303 divergent (Figure 5). These geometries have been widely examined in hillslope hydrology
304 regrading to the effects of aquifer geometry on runoff generation (Troch et al., 2003; Kong et
305 al., 2016; Luo et al., 2018). To present the results more conveniently, we placed the r - z
306 coordinate origin at the intersection of the constant-head boundary (sea or lagoon) and the
307 impermeable base, with the r -axis pointing horizontally to the internal no-flow boundary and
308 the z -axis vertically upward (Figure 5). In addition, the distance between the constant-head
309 boundary and the internal no-flow boundary (aquifer width) is denoted as L^* (Figure 5) while
310 the other parameters remain the same.

311 Following previous studies (e.g., Lu et al., 2016; 2019), different cases were selected to
312 show the effects of aquifer geometry on seawater intrusion (Cases 1 and 2 in Table 1).
313 According to Werner et al. (2017), the width of atoll islands generally varies from 100 to 1500
314 m along the radial direction. In order to focus on the effects of aquifer geometry on seawater
315 intrusion, the same L^* and L_0 were assumed for the three aquifers, with L^* and L_0 equal to
316 1000 and 200 m, respectively. Note that L_0 is the distance from the circle center to the lagoon
317 boundary for convergent aquifers, whereas it represents the distance from the circle center to
318 internal no-flow boundary for divergent aquifers hereafter. The sand characteristics were the
319 same as in the experiments of Memari et al. (2020). Two recharge events were considered

320 (Cases 1 and 2, Table 1). The freshwater-seawater interface was calculated using the
321 analytical solutions for the three different aquifers. Note that the Appendix presents analytical
322 solutions for seawater intrusion in strip aquifers deduced from Lu et al. (2019).

323 Figure 6 shows the freshwater-seawater interface calculated for Cases 1 and 2. As can be
324 seen, the extent of seawater intrusion is noticeably different for the three aquifer geometries.
325 For high recharge ($1 \times 10^{-6} \text{ m s}^{-1}$), the interface tip is located at around 500 m for the
326 divergent aquifer, which is about twice the value of the rectangular aquifer and six times the
327 value for the convergent aquifer (Figure 6a). When the recharge decreases to $3 \times 10^{-7} \text{ m s}^{-1}$,
328 the interface tip moves further landward for the three aquifers as expected, but the difference
329 between results is still great (Figure 6b). The interface tip is displaced above the aquifer bed
330 for both the rectangular and divergent aquifers, while it remains on the aquifer bed for the
331 convergent aquifer. Regardless of the recharge rate, the most landward freshwater-seawater
332 interface occurs in the divergent aquifer and vice versa for the convergent aquifer. This
333 underlines that aquifer geometry plays a major role in controlling seawater intrusion and
334 hence it is necessary to account for aquifer geometry in analyses of seawater intrusion.

335 **4.3. Sensitivity Analysis**

336 A sensitivity analysis was conducted to investigate to what extent aquifer geometry
337 affects seawater intrusion. Since we focus on the effects of aquifer geometry on the locations
338 of the freshwater-seawater interface and watertable, values of L_0 and L^* were varied, with
339 other parameters kept constant. When conducting the sensitivity analysis of L_0 , L^* was fixed
340 at 1000 m, which is a typical value for ASAs (Werner et al., 2017). Figure 7 shows the

341 sensitivity of the locations of the freshwater-seawater interface and watertable to changes in
342 L_0 (Case 3, Table 1). The freshwater-seawater interface and watertable elevation are
343 independent of L_0 for rectangular aquifers (Appendix). However, the freshwater-seawater
344 interface and watertable elevation differ greatly when varying L_0 for both convergent and
345 divergent aquifers, highlighting that L_0 plays an important role in affecting seawater intrusion.
346 Specifically, as L_0 increases, the freshwater-seawater interface moves more landward (larger
347 r/L^* , Figure 7a) and its corresponding watertable elevation decreases (Figure 7c) for
348 convergent aquifers. In contrast, for divergent aquifers increasing L_0 moves the freshwater-
349 seawater interface more seaward (smaller r/L^* , Figure 7b) and its corresponding watertable
350 elevation increases (Figure 7d). For a given L_0 , divergent aquifers have the largest extent of
351 seawater intrusion and the lowest watertable elevation, and conversely for convergent aquifers
352 (Figure 7).

353 Regardless of the freshwater-seawater interface and watertable elevation, the deviation
354 between rectangular aquifers and divergent or convergent aquifers is significant when L_0 is
355 less than 2000 m (Figure 7). For example, the r -coordinate of the interface tip ($z = 0$) is 262 m
356 for the rectangular aquifer at $L_0 = 200$ m, whereas it is 78 (31% of that in the rectangular
357 aquifer) and 500 m (191% of that in the rectangular aquifer) for the convergent and divergent
358 aquifers, respectively. As L_0 increases, the deviation between the three aquifers decreases.
359 When $L_0 = 2000$ m, the r -coordinate of the interface tip is 262, 209 (80% of that in the
360 rectangular aquifer) and 318 m (121% of that in the rectangular aquifer) for the rectangular,
361 convergent and divergent aquifers, respectively. As L_0 increases to 6000 m, the freshwater-

362 seawater interface and watertable elevation of both convergent and divergent aquifers tend to
363 those of rectangular aquifers, i.e., geometry effects decrease with increasing L_0 . These results
364 highlight the critical role played by the shape of aquifers. As a result, ignoring the aquifer
365 geometry may lead to an inappropriate management strategy for groundwater resources in
366 atoll islands.

367 The sensitivity of the freshwater-seawater interface and watertable elevation to L^* was
368 investigated by varying L^* from 600 to 1600 m while fixing L_0 to 200 m (Case 4, Table 1). As
369 shown in Figure 8, contrary to the results for varying L_0 , in this case the freshwater-seawater
370 interface and watertable elevation in all three topographies are related to L^* . Again, the extent
371 of seawater intrusion is greatest in divergent aquifers and least in convergent aquifers for
372 given L^* . When L^* increases, the freshwater-seawater interface moves seaward and the
373 watertable elevation increases, regardless of aquifer geometry, i.e., the seawater intrusion
374 decreases (Figures 8a-c). This is because the total freshwater flux increases with increasing
375 L^* , leading to a higher hydraulic gradient and hence less seawater intrusion (Figures 8d-f).
376 Moreover, an increase in L^* reduces the differences in the seawater intrusion distance among
377 the three geometries, i.e., the effects of aquifer geometry on seawater intrusion are more
378 significant at small L^* . However, even at the maximum L^* considered (1600 m), the deviation
379 between three aquifers remains significant: The r -coordinate of the interface tip is about 148
380 m for the rectangular aquifer, whereas it is about 32 (22% of that in the rectangular aquifer)
381 and 278 m (188% of that in the rectangular aquifer) for the convergent and divergent aquifers,
382 respectively. Both L_0 and L^* can greatly impact seawater intrusion estimates for divergent and

383 convergent aquifers, highlighting the necessity to include geometry effects in analytical
384 solutions of seawater intrusion.

385 **5. Conclusions**

386 Based on the Ghijben-Herzberg and hillslope-storage Boussinesq equations, we derived
387 analytical solutions of steady-state seawater intrusion for ASAs, with a focus on the
388 freshwater-seawater interface and its corresponding watertable elevation as affected by
389 recharge. After comparing with experimental data of Memari et al. (2020), the analytical
390 solutions were employed to examine the effects of aquifer geometry on seawater intrusion in
391 island aquifers. Three different shapes of island aquifer were compared: convergent,
392 rectangular and divergent. The results lead to the following conclusions:

- 393 • The presented analytical solutions perform well in predicting the experimental freshwater-
394 seawater interface, suggesting that these analytical solutions can predict seawater intrusion
395 reasonably in different aquifer geometries.
- 396 • Island geometry plays a significant role in affecting the freshwater-seawater interface and
397 watertable elevation. Other factors being equal, the extent of seawater intrusion is greatest
398 in divergent aquifers, and conversely least in convergent aquifers. In contrast, the
399 watertable elevation is lowest in divergent aquifers and highest in convergent aquifers.
- 400 • The effects of aquifer geometry on seawater intrusion are dependent on the aquifer width
401 and distance from the circle center to the internal no-flow boundary (Figures 7 and 8). A
402 larger aquifer width and distance from the circle center to the inner arc (the lagoon
403 boundary for convergent aquifers or the internal no-flow boundary for divergent aquifers)

404 weaken the role played by aquifer geometry and hence lead to a smaller deviation of the
405 extent of seawater intrusion between the three topographies.

406 Real island aquifers are expected to exhibit more complexity than considered here, e.g.,
407 they will have more complex shapes and are subjected to transient flow conditions caused by
408 tides, waves and groundwater pumping (Mantoglou et al. 2003; Pool & Carrera., 2011;
409 Werner et al., 2013). In addition, since the experimental scale of Memari et al. (2020) is
410 necessarily small, future experiments and field data are needed to further validate and
411 facilitate the analytical solutions. Despite this, the new analytical solutions, validated against
412 experiments, can be used as a tool for rapid estimation of seawater intrusion in ASAs once
413 known island geometry and corresponding soil properties are given.

414 **Appendix: Analytical Solutions for Rectangular Aquifers**

415 For rectangular aquifers, the seawater intrusion in Unit 1 is identical to that in Unit 2
 416 because of symmetry. With the interface tip on the aquifer bed, analytical solutions for the
 417 freshwater-seawater interface (h_s), watertable elevation (h), and r -coordinate of the interface
 418 tip in Unit 2 (r_{t2}) can be respectively written as (Lu et al., 2019),

$$419 \quad h_s = \alpha \sqrt{\frac{N}{(1+\alpha)K_s} \left(\frac{L^2}{4} - r^2 \right)} \quad (\text{A1})$$

$$420 \quad h = \begin{cases} \sqrt{\frac{N}{K_s} (r_{t2}^2 - r^2) + \left(\frac{H_s}{\alpha} + H_s \right)} & 0 \leq r \leq r_{t2} \\ \sqrt{\frac{N}{(1+\alpha)K_s} \left(\frac{L^2}{4} - r^2 \right) + H_s} & r_{t2} < r \leq \frac{L}{2} \end{cases} \quad (\text{A2})$$

$$421 \quad r_{t2} = \sqrt{\frac{L^2}{4} - \frac{(1+\alpha)K_s}{N} \left(\frac{H_s^2}{\alpha^2} \right)} \quad (\text{A3})$$

422 When the interface tip is above the aquifer bed, the analytical solution for the freshwater-
 423 seawater interface location and watertable elevation in Unit 2 are the same as equations (A1)
 424 and (A2), respectively.

425 **Code/Data availability**

426 Experimental data used in this study were compiled from Memari et al. (2020).

427 **Author contributions**

428 All authors contributed to the design of the research. ZL carried out data collation,
429 developed the analytical solutions and prepared the manuscript with contributions from all
430 co-authors. All authors contributed to the interpretation of the results and provided feedback.

431 **Competing interests**

432 The authors declare that they have no conflicts of interest.

433 **Acknowledgments**

434 This research was supported by the National Key R&D Program of China
435 (2019YFC0409004) and the National Natural Science Foundation of China (51979095 and
436 41807178). ZL acknowledges EPFL for financial support and JK acknowledges the Qing Lan
437 Project of Jiangsu Province (2020). We appreciate the constructive comments from the
438 handling Editor Mauro Giudici and three anonymous reviewers, which led to significant
439 improvement of the paper.

440 **References**

441 Ayers, J. F., & Vacher, H. L. (1986). Hydrogeology of an atoll island: A conceptual model
442 from detailed study of a Micronesian example. *Groundwater*, 24(2), 185-198.

443 <https://doi.org/10.1111/j.1745-6584.1986.tb00994.x>

444 Bailey, R. T., Jenson, J. W., & Olsen, A. E. (2010). Estimating the ground water resources of
445 atoll islands. *Water*, 2(1), 1-27. <https://doi.org/10.3390/w2010001>

446 Bailey, R. T., Jenson, J. W., & Olsen, A. E. (2009). Numerical modeling of atoll island
447 hydrogeology. *Groundwater*, 47(2), 184-196. <https://doi.org/10.1111/j.1745->

448 [6584.2008.00520.x](https://doi.org/10.1111/j.1745-6584.2008.00520.x)

449 Bedekar, V. S., Memari, S. S., & Clement, T. P. (2019). Investigation of transient freshwater
450 storage in island aquifers. *Journal of Contaminant Hydrology*, 221, 98-107.

451 <https://doi.org/10.1016/j.jconhyd.2019.02.004>

452 Chesnaux, R., & Allen, D. M. (2008). Groundwater travel times for unconfined island
453 aquifers bounded by freshwater or seawater. *Hydrogeology Journal*, 16(3), 437-445.

454 <https://doi.org/10.1007/s10040-007-0241-6>

455 Dose, E. J., Stoeckl, L., Houben, G. J., Vacher, H. L., Vassolo, S., Dietrich, J., &

456 Himmelsbach, T. (2014). Experiments and modeling of freshwater lenses in layered
457 aquifers: Steady state interface geometry. *Journal of Hydrology*, 509, 621-630.

458 <https://doi.org/10.1016/j.jhydrol.2013.10.010>

459 Drabbe J. & Badon Ghijben, W. (1889). *Nota in verband met de voorgenomen put boring*
460 *nabij Amsterdam*. Tijdschrift van het Koninklijk Instituut van Ingenieurs. pp. 8-22,

461 Gravenhage, Netherlands.

462 Duvat, V. K. E. (2019). A global assessment of atoll island planform changes over the past
463 decades. *Wiley Interdisciplinary Reviews: Climate Change*, 10(1), e557.
464 <https://doi.org/10.1002/wcc.557>

465 Fan, Y., & Bras, R. L. (1998). Analytical solutions to hillslope subsurface storm flow and
466 saturation overland flow. *Water Resources Research*, 34(4), 921-927.
467 <https://doi.org/10.1029/97WR03516>

468 Fetter, C. W. (1972). Position of the saline water interface beneath oceanic islands. *Water
469 Resources Research*, 8(5), 1307-1315. <https://doi.org/10.1029/WR008i005p01307>

470 Gingerich, S. B., Voss, C. I., & Johnson, A. G. (2017). Seawater-flooding events and impact
471 on freshwater lenses of low-lying islands: Controlling factors, basic management and
472 mitigation. *Journal of Hydrology*, 551, 676-688.
473 <https://doi.org/10.1016/j.jhydrol.2017.03.001>

474 Greskowiak, J., Röper, T., & Post, V. E. (2013). Closed-form approximations for two-
475 dimensional groundwater age patterns in a fresh water lens. *Groundwater*, 51(4), 629-
476 634. <https://doi.org/10.1111/j.1745-6584.2012.00996.x>

477 Hazenberg, P., Fang, Y., Broxton, P., Gochis, D., Niu, G. Y., Pelletier, J. D., Troch., P. A., &
478 Zeng, X. (2015). A hybrid-3D hillslope hydrological model for use in Earth system
479 models. *Water Resources Research*, 51(10), 8218-8239.
480 <https://doi.org/10.1002/2014WR016842>

481 Hazenberg, P., Broxton, P., Gochis, D., Niu, G. Y., Pangle, L. A., Pelletier, J. D., Troch., P. A.,

482 & Zeng, X. (2016). Testing the hybrid-3-D hillslope hydrological model in a
483 controlled environment. *Water Resources Research*, 52(2), 1089-1107.
484 <https://doi.org/10.1002/2015WR018106>

485 Herzberg, A. (1901). Die wasserversorgung einiger Nordseebäder. *Journal für*
486 *Gasbeleuchtung und Wasserversorgung*, 44, 815-819, 45, 842-844.

487 Hilberts, A. G. J., Troch, P. A., & Paniconi, C. (2005). Storage-dependent drainable porosity
488 for complex hillslopes. *Water Resources Research*, 41(6), W06001.
489 <https://doi.org/10.1029/2004WR003725>

490 Hilberts, A. G., Troch, P. A., Paniconi, C., & Boll, J. (2007). Low-dimensional modeling of
491 hillslope subsurface flow: Relationship between rainfall, recharge, and unsaturated
492 storage dynamics. *Water Resources Research*, 43(3), W03445.
493 <https://doi.org/10.1029/2006WR004964>

494 Ketabchi, H., Mahmoodzadeh, D., Ataie-Ashtiani, B., Werner, A. D., & Simmons, C. T.
495 (2014). Sea-level rise impact on fresh groundwater lenses in two-layer small islands.
496 *Hydrological Processes*, 28(24), 5938-5953. <https://doi.org/10.1002/hyp.10059>

497 Kong, J., Shen, C., Luo, Z., Hua, G., & Zhao, H. (2016). Improvement of the hillslope-storage
498 Boussinesq model by considering lateral flow in the unsaturated zone. *Water*
499 *Resources Research*, 52(4), 2965-2984. <https://doi.org/10.1002/2015WR018054>

500 Lam, R. K. (1974). Atoll permeability calculated from tidal diffusion. *Journal of Geophysical*
501 *Research*, 79(21), 3073-3081. <https://doi.org/10.1029/JC079i021p03073>

502 Liu, J., & Tokunaga, T. (2019). Future risks of tsunami-induced seawater intrusion into

503 unconfined coastal aquifers: Insights from numerical simulations at Niijima Island,
504 Japan. *Water Resources Research*, 55(12), 10082-10104.
505 <https://doi.org/10.1029/2019WR025386>

506 Liu, Y., X. Mao, J. Chen, and D. A. Barry. 2014. Influence of a coarse interlayer on seawater
507 intrusion and contaminant migration in coastal aquifers. *Hydrological Processes*, 28(20),
508 5162-5175. <https://dx.doi.org/10.1002/hyp.10002>

509 Lu, C., Cao, H., Ma, J., Shi, W., Rathore, S. S., Wu, J., & Luo, J. (2019). A proof-of-concept
510 study of using a less permeable slice along the shoreline to increase fresh groundwater
511 storage of oceanic islands: Analytical and experimental validation. *Water Resources*
512 *Research*, 55(8), 6450-6463. <https://doi.org/10.1029/2018WR024529>

513 Lu, C., Xin, P., Kong, J., Li, L., & Luo, J. (2016). Analytical solutions of seawater intrusion in
514 sloping confined and unconfined coastal aquifers. *Water Resources Research*, 52(9),
515 6989-7004. <https://doi.org/10.1002/2016WR019101>

516 Luo, Z., Shen, C., Kong, J., Hua, G., Gao, X., Zhao, Z., Zhao, H., & Li, L. (2018). Effects of
517 unsaturated flow on hillslope recession characteristics. *Water Resources Research*,
518 54(3), 2037-2056. <https://doi.org/10.1002/2017WR022257>

519 Mantoglou, A. (2003). Pumping management of coastal aquifers using analytical models of
520 saltwater intrusion. *Water Resources Research*, 39(12), 1335.
521 <https://doi.org/10.1029/2002WR001891>

522 Memari, S. S., Bedekar, V. S., & Clement, T. P. (2020). Laboratory and numerical
523 investigation of saltwater intrusion processes in a circular island aquifer. *Water*

524 *Resources Research*, 56(2), e2019WR025325. <https://doi.org/10.1029/2019WR025325>

525 Morgan, L. K., & Werner, A. D. (2014). Seawater intrusion vulnerability indicators for
526 freshwater lenses in strip islands. *Journal of Hydrology*, 508, 322-327.
527 <https://doi.org/10.1016/j.jhydrol.2013.11.002>

528 Paniconi, C., Troch, P. A., Van Loon, E. E., & Hilberts, A. G. (2003). Hillslope-storage
529 Boussinesq model for subsurface flow and variable source areas along complex
530 hillslopes: 2. Intercomparison with a three-dimensional Richards equation model.
531 *Water Resources Research*, 39(11), 1317. <https://doi.org/10.1029/2002WR001730>

532 Pool, M., & Carrera, J. (2011). A correction factor to account for mixing in Ghyben-Herzberg
533 and critical pumping rate approximations of seawater intrusion in coastal aquifers.
534 *Water Resources Research*, 47(5), W05506. <https://doi.org/10.1029/2010WR010256>

535 Post, V. E. (2018). Annotated translation of “Nota in verband met de voorgenomen putboring
536 nabij Amsterdam [Note concerning the intended well drilling near Amsterdam]” by J.
537 Drabbe and W. Badon Ghijben (1889). *Hydrogeology Journal*, 26(6), 1771-1788.
538 <https://doi.org/10.1007/s10040-018-1797-z>

539 Post, V. E. A., Houben, G. J., Stoeckl, L., & Sültenfuß, J. (2019). Behaviour of tritium and
540 tritiogenic helium in freshwater lens groundwater systems: Insights from Langeoog
541 Island, Germany. *Geofluids*, Volume 2019, Article ID 1494326.
542 <https://doi.org/10.1155/2019/1494326>

543 Röper, T., Greskowiak, J., Freund, H., & Massmann, G. (2013). Freshwater lens formation
544 below juvenile dunes on a barrier island (Spiekeroog, Northwest Germany). *Estuarine*,

545 *Coastal and Shelf Science*, 121-122, 40-50. <https://doi.org/10.1016/j.ecss.2013.02.004>

546 Stoeckl, L., Houben, G. J., & Dose, E. J. (2015). Experiments and modeling of flow processes
547 in freshwater lenses in layered island aquifers: Analysis of age stratification, travel
548 times and interface propagation. *Journal of Hydrology*, 529, 159-168.
549 <https://doi.org/10.1016/j.jhydrol.2015.07.019>

550 Storlazzi, C. D., Gingerich, S. B., van Dongeren, A., Cheriton, O. M., Swarzenski, P. W.,
551 Quataert, E., Voss, C. I., Field, D. W., Annamalai, H., Piniak, G. A., & McCall, R.
552 (2018). Most atolls will be uninhabitable by the mid-21st century because of sea-level
553 rise exacerbating wave-driven flooding. *Science Advances*, 4(4), eaap9741.
554 <https://doi.org/10.1126/sciadv.aap9741>

555 Strack, O. D. L. (1976). A single-potential solution for regional interface problems in coastal
556 aquifers. *Water Resources Research*, 12(6), 1165-1174.
557 <https://doi.org/10.1029/WR012i006p01165>

558 Stuyfzand, P. J. (2017). Observations and analytical modeling of freshwater and rainwater
559 lenses in coastal dune systems. *Journal of Coastal Conservation*, 21(5), 577-593.
560 <https://doi.org/10.1007/s11852-016-0456-6>

561 Stuyfzand, P. J. (1993). *Hydrochemistry and hydrology of the coastal dune area of the Western*
562 *Netherlands*. Ph.D. Thesis. Vrije University, Amsterdam, KIWA, ISBN 90-74741-01-
563 0. <http://dare.uvu.vu.nl/handle/1871/12716>

564 Thomas, A., Baptiste, A., Martyr-Koller, R., Pringle, P., & Rhiney, K. (2020). Climate change
565 and small island developing states. *Annual Review of Environment and Resources*,

566 45(1), 1-27. <https://doi.org/10.1146/annurev-environ-012320-083355>

567 Troch, P. A., Paniconi, C., & Emiel van Loon, E. (2003). Hillslope-storage Boussinesq model
568 for subsurface flow and variable source areas along complex hillslopes: 1.
569 Formulation and characteristic response. *Water Resources Research*, 39(11), 1316.
570 <https://doi.org/10.1029/2002WR001728>

571 Underwood, M. R., Peterson, F. L., & Voss, C. I. (1992). Groundwater lens dynamics of atoll
572 islands. *Water Resources Research*, 28(11), 2889-2902.
573 <https://doi.org/10.1029/92WR01723>

574 Vacher, H. L. 1988. Dupuit-Ghyben-Herzberg analysis of strip-island lenses. *Geological*
575 *Society of America Bulletin*, 100, 580-591. [https://doi.org/10.1130/0016-](https://doi.org/10.1130/0016-7606(1988)100<0580:DGHAOS>2.3.CO;2)
576 [7606\(1988\)100<0580:DGHAOS>2.3.CO;2](https://doi.org/10.1130/0016-7606(1988)100<0580:DGHAOS>2.3.CO;2)

577 Werner, A. D., Sharp, H. K., Galvis, S. C., Post, V. E., & Sinclair, P. (2017). Hydrogeology
578 and management of freshwater lenses on atoll islands: Review of current knowledge
579 and research needs. *Journal of Hydrology*, 551, 819-844.
580 <https://doi.org/10.1016/j.jhydrol.2017.02.047>

581 Werner, A. D., Bakker, M., Post, V. E., Vandenbohede, A., Lu, C., Ataie-Ashtiani, B.,
582 Simmons, C. T., & Barry, D. A. (2013). Seawater intrusion processes, investigation
583 and management: Recent advances and future challenges. *Advances in Water*
584 *Resources*, 51, 3-26. <https://doi.org/10.1016/j.advwatres.2012.03.004>

585 Werner, A. D., & Simmons, C. T. (2009). Impact of sea-level rise on sea water intrusion in
586 coastal aquifers. *Groundwater*, 47(2), 197-204. <https://doi.org/10.1111/j.1745->

587 [6584.2008.00535.x](#)

588 White, I., & Falkland, T. (2010). Management of freshwater lenses on small Pacific islands.

589 *Hydrogeology Journal*, 18(1), 227-246. <https://doi.org/10.1007/s10040-009-0525-0>

590 Zhang, Y., Li, L., Erler, D. V., Santos, I., & Lockington, D. (2016). Effects of alongshore

591 morphology on groundwater flow and solute transport in a nearshore aquifer. *Water*

592 *Resources Research*, 52(2), 990-1008. <https://doi.org/10.1002/2015WR017420>

593

Table 1. List of parameters use in different simulations.

	No.	L^* (m)	L_0 (m)	H_s (m)	d (m)	α (-)	K_s (m s ⁻¹)	N (m s ⁻¹)
Cases	1	1000	200	38	45	40	1.23×10^{-2}	1×10^{-6}
	2	1000	200	38	45	40	1.23×10^{-2}	3×10^{-7}
	3	1000	†	38	45	40	1.23×10^{-2}	1×10^{-6}
	4	†	200	38	45	40	1.23×10^{-2}	1×10^{-6}

594

†The parameter is varied: The range of L_0 is from 200 to 6000 m, whereas the range of L^* is

595

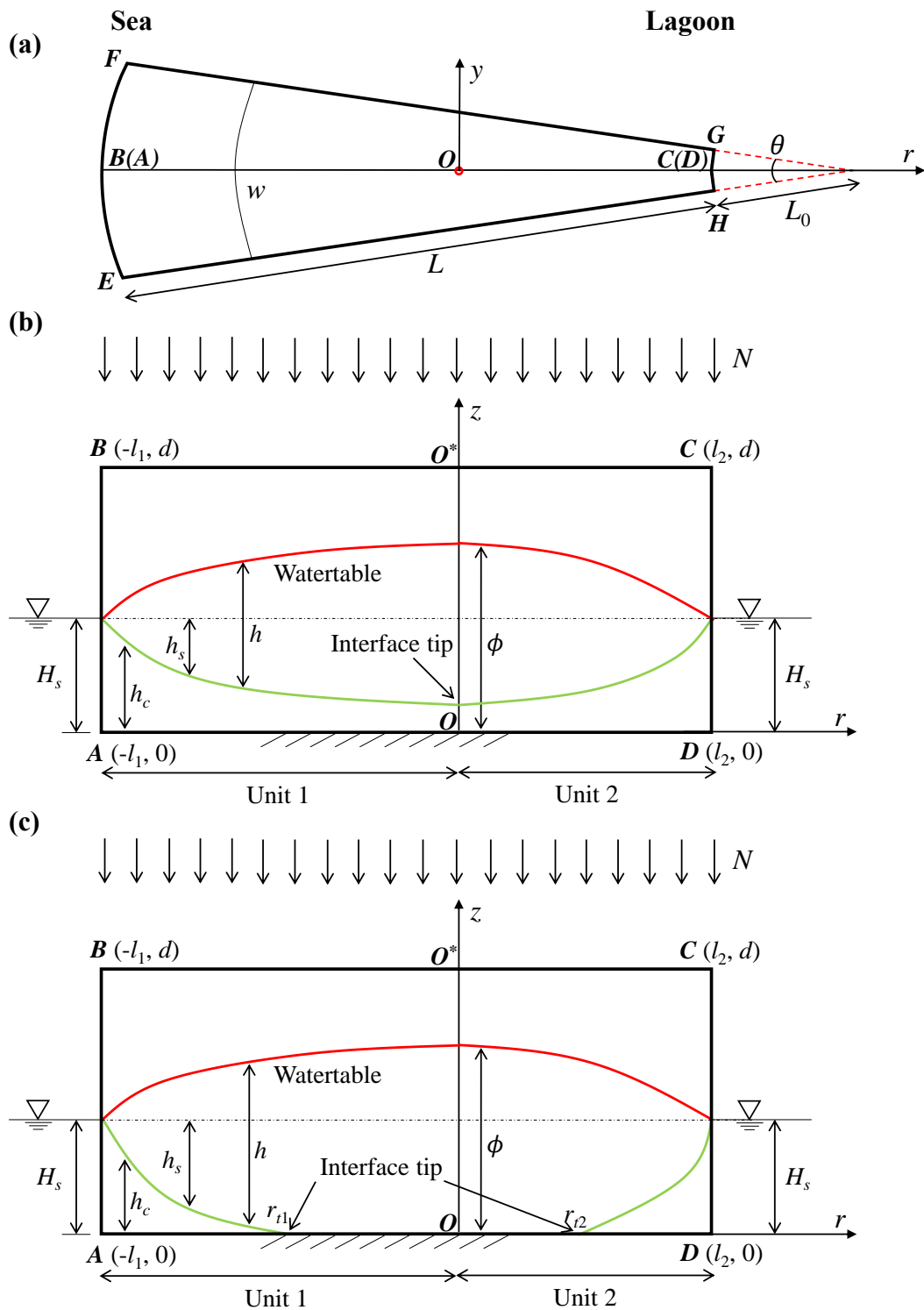
from 600 to 1600 m.



596

597 **Figure 1.** Island with an annulus segment in the Namu Atoll, Marshall Islands (© Google

598 Earth).



599

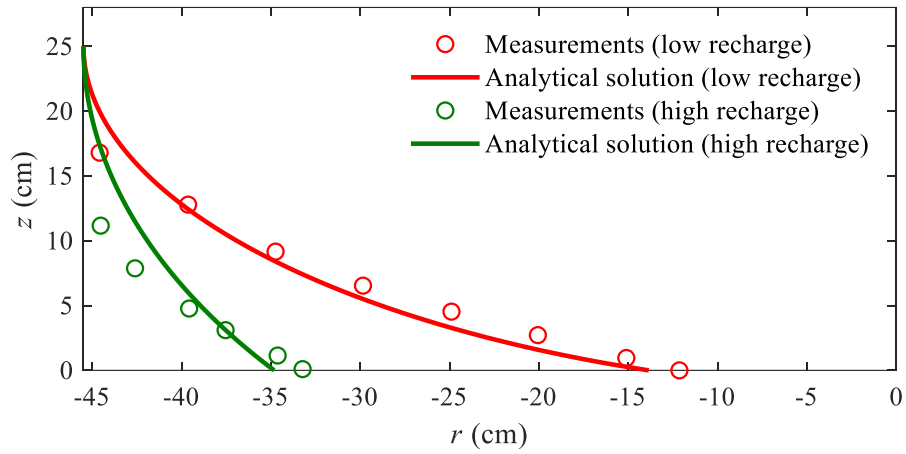
600 **Figure 2.** Conceptual model of an annulus segment aquifer (a slice of an atoll island). (a) Plan

601 view and (b, c) lateral vertical cross section with the saltwater interface tip (b) above the

602 aquifer bed (single location) and (c) on the aquifer bed (two locations). In (a), the sea

603 boundary is on EF and the atoll lagoon boundary is on HG ; In (b) and (c), AD is the

604 impermeable base and OO^* is the internal no-flow boundary.



605

606

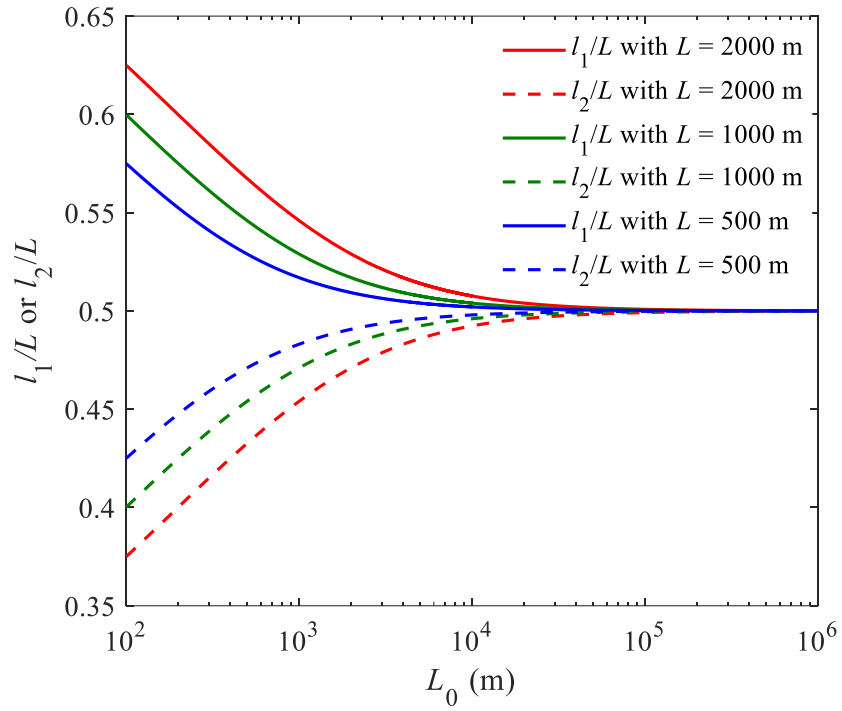
Figure 3. Comparison between analytical and experimental (data compiled from Memari et

607

al., 2020) results for the freshwater-seawater interface location for different recharge events.

608

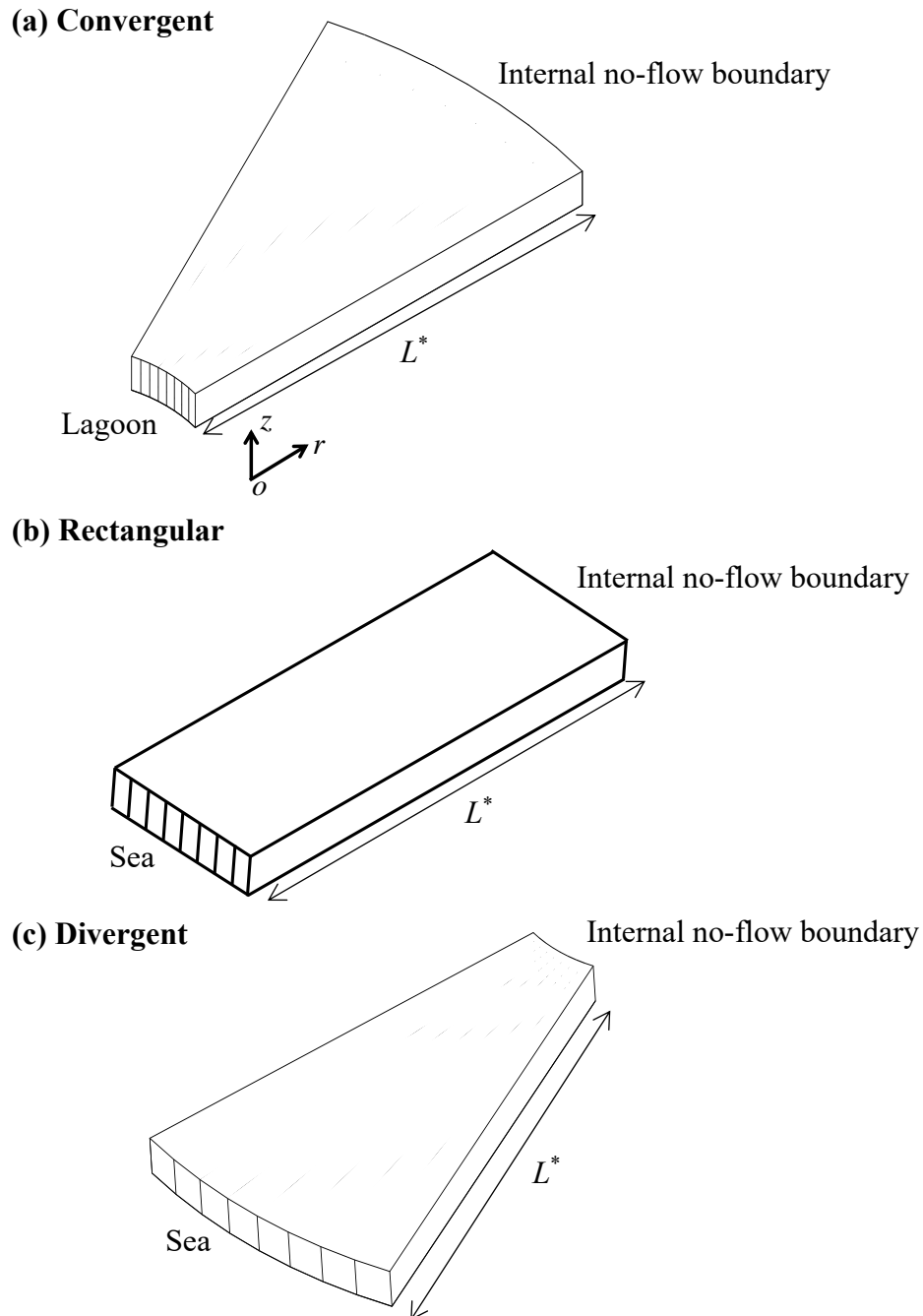
Note that the left and right sides are the sea and internal no-flow boundaries, respectively.



609

610

Figure 4. Widths of Unit 1 and Unit 2 versus L_0 for aquifers with different total width L .

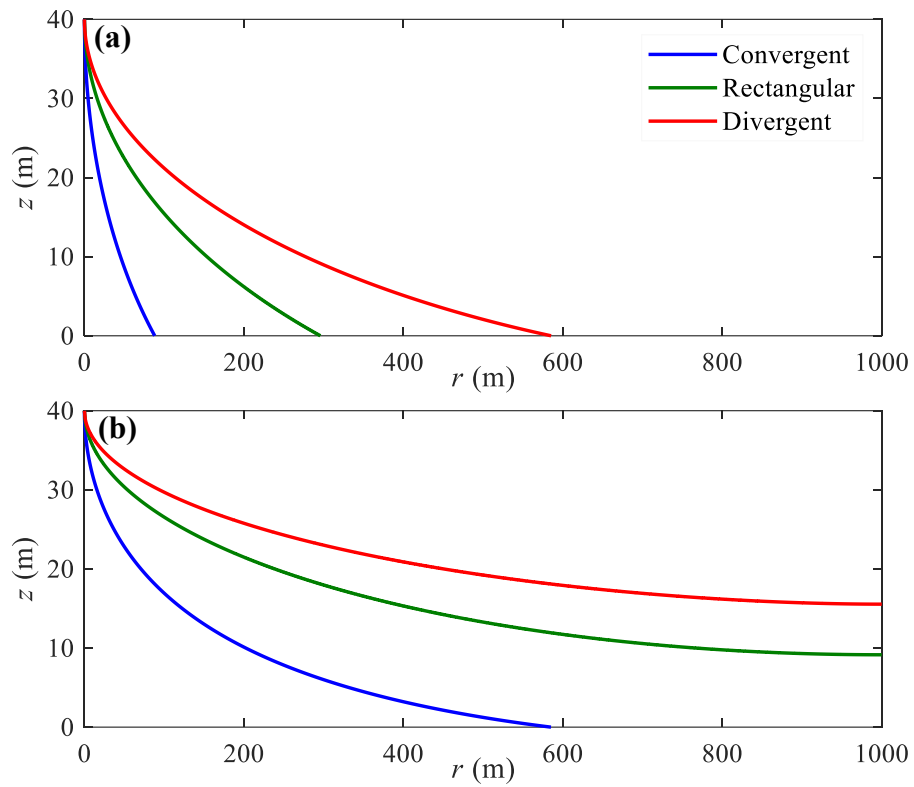


611

612

613

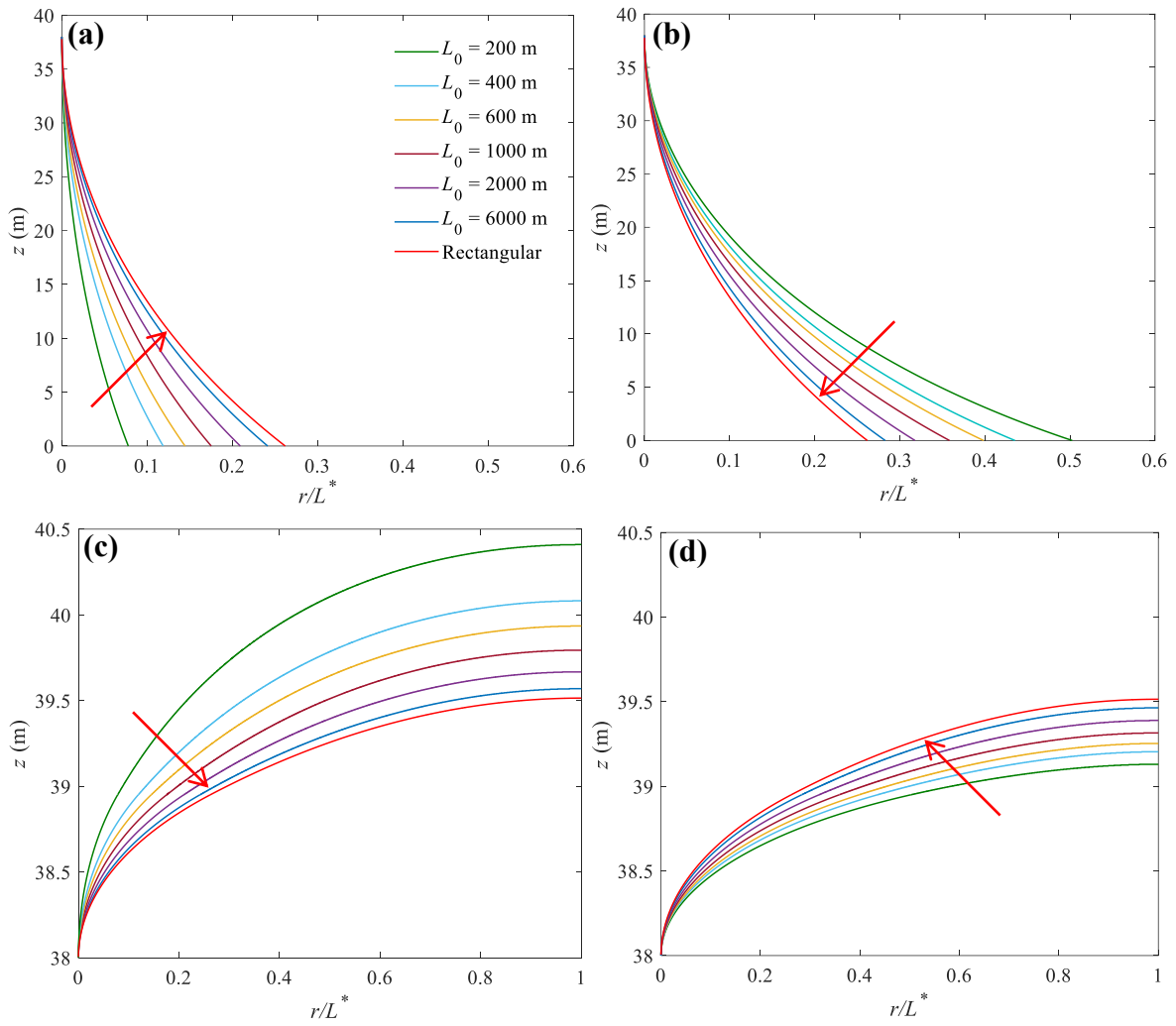
614 **Figure 5.** Three-dimensional view of (a) convergent (smaller side facing the lagoon), (b)
 615 rectangular and (c) divergent aquifers (larger side facing the sea) compared in this study. L^*
 616 represents the distance from the sea/lagoon to the internal no-flow boundary, i.e., l_1 or l_2 in
 617 Figure 2. The internal no-flow boundary corresponds to the z -axis in Figure 2.



618

619

620 **Figure 6.** Freshwater-seawater interface predicted by analytical solutions for three different
 621 aquifers with (a) high and (b) low recharge (Cases 1 and 2 in Table 1). Note that $r = 1000$ m is
 622 the internal no-flow boundary in Figure 5.



623

624

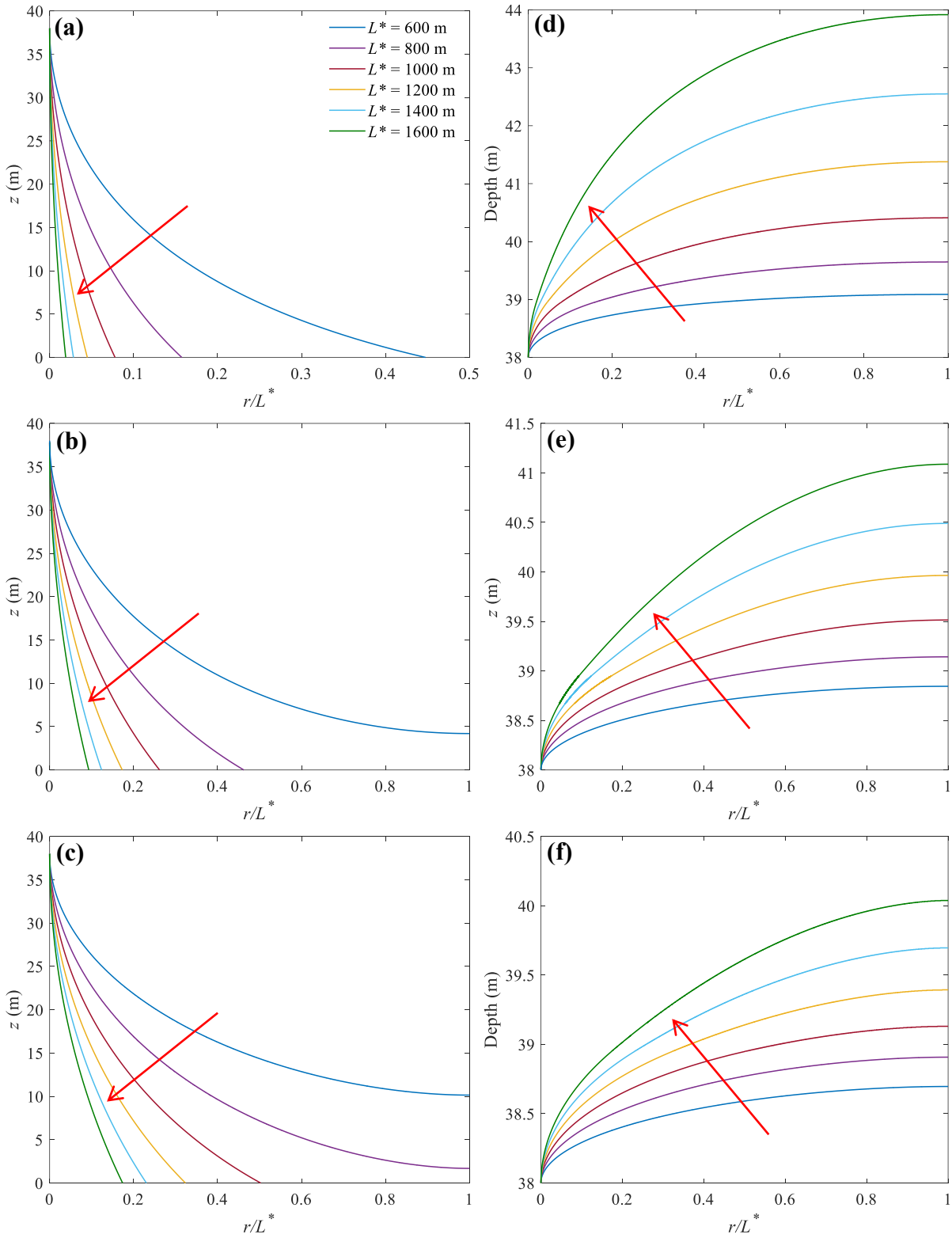
625

626

627

628

Figure 7. Sensitivity of (a, b) the locations of the freshwater-seawater interface and (c, d) watertable to L_0 for convergent (left panel) and divergent (right panel) aquifers. The arrow in each plot shows the direction of increasing L_0 (values given in (a), used to produce the different curves). Note that predictions for rectangular aquifers are independent of L_0 .



629

630

631

632

633

634

Figure 8. Sensitivity of (a-c) the locations of the freshwater-seawater interface and (d-f)

watertable to L^* for convergent (a, d), rectangular (b, e) and divergent (c, f) aquifers. The

arrow in each plot points to the increase of L^* values used to construct each curve (values

635 indicated in (a)).